

Targeting SARS-CoV-2 M3CLpro by HCV NS3/4a Inhibitors: *In Silico* Modeling and *In Vitro* Screening

Anjela Manandhar, Benjamin E. Blass, Dennis J. Colussi, Imane Almi, Magid Abou-Gharbia, Michael L. Klein, and Khaled M. Elokely*



Cite This: <https://dx.doi.org/10.1021/acs.jcim.0c01457>



Read Online

ACCESS |



Metrics & More

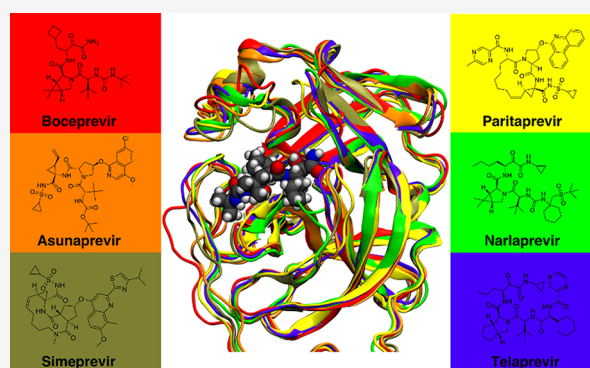


Article Recommendations



Supporting Information

ABSTRACT: Currently the entire human population is in the midst of a global pandemic caused by SARS-CoV-2 (Severe Acute Respiratory Syndrome Coronavirus 2). This highly pathogenic virus has to date caused >71 million infections and >1.6 million deaths in >180 countries. Several vaccines and drugs are being studied as possible treatments or prophylactics of this viral infection. M3CLpro (coronavirus main cysteine protease) is a promising drug target as it has a significant role in viral replication. Here we use the X-ray crystal structure of M3CLpro in complex with boceprevir to study the dynamic changes of the protease upon ligand binding. The binding free energy was calculated for water molecules at different locations of the binding site, and molecular dynamics (MD) simulations were carried out for the M3CLpro/boceprevir complex, to thoroughly understand the chemical environment of the binding site. Several HCV NS3/4a protease inhibitors were tested *in vitro* against M3CLpro. Specifically, asunaprevir, narlaprevir, paritaprevir, simeprevir, and telaprevir all showed inhibitory effects on M3CLpro. Molecular docking and MD simulations were then performed to investigate the effects of these ligands on M3CLpro and to provide insights into the chemical environment of the ligand binding site. Our findings and observations are offered to help guide the design of possible potent protease inhibitors and aid in coping with the COVID-19 pandemic.



INTRODUCTION

The novel coronavirus SARS-CoV-2 (Severe Acute Respiratory Syndrome Coronavirus 2) is a highly infectious, positive sense RNA virus that is responsible for the present outbreak of COVID-19.¹ This virus first appeared in Wuhan, China, in December 2019^{2,3} and has caused a global pandemic the likes of which has not been seen since the 1918 Spanish flu.⁴ The World Health Organization (WHO) declared the outbreak a pandemic.⁵ Health care systems across the globe were pushed to their limits, and countries instituted strict lockdowns in an effort to slow the virus's spread. The United States alone accounted for >1.6 million cases and around 300 000 COVID-19 deaths. Importantly, although several viable vaccine options have now emerged for treatment and prevention, current drug therapeutic options to address this new pathogen are limited at best.

A detailed understanding of SARS-CoV-2 pathophysiology is still being developed, but the genetic makeup of this virus has been elucidated and several potential drug targets have been identified. These include an RNA-dependent RNA polymerase (RDRp), the spike protein (S protein), transmembrane protease serine 2 (TMPRSS2), angiotensin-converting enzyme 2 (ACE2), angiotensin AT2 receptor

(AT2), a papain-like protease (PLpro), and the coronavirus main cysteine protease (M3CLpro).^{2,6–11} To date, only one antiviral agent, remdesivir (Veklury (1), Figure 1), has been approved by the FDA for the treatment of SARS-CoV-2 infection based on the nonconclusive results of a phase III clinical trial of shortening the average patient hospitalization stay by 4 days, but there was no change in patient mortality.^{12,13} The value of this drug for the treatment of SARS-CoV-2 infection remains unclear with recent study suggesting the efficacy of remdesivir in selective patients.¹⁴ Remdesivir treatment for COVID-19 patients with a rare autoimmune disorder had dramatic improvement of the symptoms with eradication of the virus. In addition, it remains to be determined if serious side effects will emerge as this new drug becomes more widely distributed. The risk of remdesivir-resistant strains of SARS-CoV-2 also remains

Received: December 18, 2020



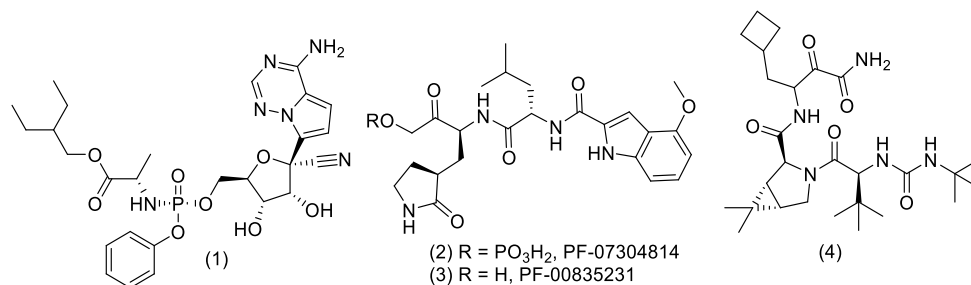


Figure 1. Remdesivir (1), Pfizer M3CLpro inhibitor (2) and prodrug thereof (3), and boceprevir (4).

unknown. Additional therapeutics that target SARS-CoV-2 through an alternate mechanism would provide an opportunity to use combination therapies, an approach successfully used to treat human immunodeficiency virus (HIV)^{15–17} and hepatitis C (HCV).^{18,19} In both cases, combination therapies employing agents with different mechanisms provided improved viral clearance and limited the possibility of drug resistance.

As part of our effort to address the COVID-19 crisis and provide clinicians with access to therapies with multiple mechanisms of action, thereby enabling combination therapies, we have initiated a program to develop novel M3CLpro inhibitors. This essential cysteine protease is responsible for cleavage of at least 11 sites on the large polyprotein 1ab (replicase 1ab, ~790 kDa) that in most instances targets the recognition sequence Leu-Gln-(Ser, Ala, Gly).^{21,22} X-ray crystal data (PDB 6Y2E, Figure 2) show that

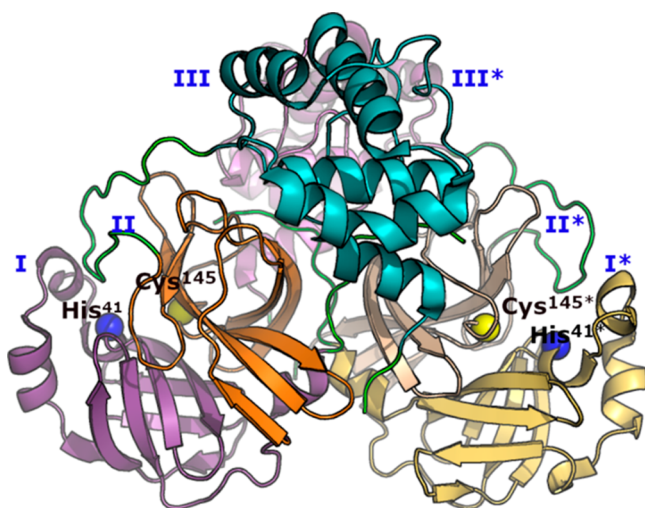


Figure 2. M3CLpro crystal structure (PDB 6Y2E). The three regions of each monomer are labeled and color coded. The key active site residues His⁴¹ and Cys¹⁴⁵ are shown as spheres. The color scheme is purple (I), orange (II), and cyan (III) for chain A and yellow (I*), wheat (II*), and violet (III*) for chain B. The image was prepared using PyMOL.²⁰

this enzyme is composed of three domains.²² Domain I is a chymotrypsin-like region (residues 10–99), while domain II is a picornavirus 3C protease-like region (residues 100–182). These domains contain six-stranded antiparallel β -barrels that together form the enzyme's active site. The last region, domain III (residues 198–303), is a globular grouping of five helices that regulate dimerization of the enzyme through the formation of a salt bridge between Arg⁴ of one monomer and

Glu²⁹⁰ of a second monomer.²³ Dimerization establishes a perpendicular orientation of the two monomers in which domain II of one monomer interacts with the NH₂ terminus (N-finger) of the other monomer over an ~1394 Å² contact interface. This interaction allows the N-finger of one monomer to interact with Glu¹⁶⁶ of the other, which shapes the S1 pocket of the active site.²⁴ In the absence of dimerization, catalytic activity is limited.²³

Similar to other cysteine proteases,²⁵ M3CLpro cleaves its target using a Cys/His catalytic dyad, in this case Cys¹⁴⁵ and His⁴¹. In this process, the thiol of Cys¹⁴⁵ is deprotonated by His⁴¹, which facilitates its nucleophilic attack on the amide carbonyl of the target peptide. Collapse of the transient tetrahedral intermediate ejects the NH₂-fragment peptide and produces a Cys¹⁴⁵ thioester, which is readily cleaved by water to release the CO₂H fragment. This readies the active site for the next substrate. To date, there are no FDA approved therapies that target M3CLpro for the treatment of SARS-CoV-2 infection and there are no ongoing clinical trials of lead compounds that target this enzyme. Only one company, Pfizer, has published results in this area. They recently reported the discovery of PF-07304814 (2), a prodrug of the active agent PF-00835231 (3) (Figure 1), that inhibits M3CLpro. Pfizer described this compound as a potential clinical candidate, but as of December 2020, clinical trials have not begun.²⁶ There remains a clear and compelling need for COVID-19 therapies and novel clinical candidates targeting M3CLpro.

Given the urgency of the current situation, several research groups are using *in silico* studies and *in vitro* assays to examine approved drugs as inhibitors of M3CLpro. For example, Ghahremanpour et al.²⁷ tested a library of ca. 2000 drugs against M3CLpro. Fourteen drugs significantly reduced M3CLpro activity at a concentration of 100 μ M, and specifically manidipine, boceprevir, lercanidipine, bedaquiline, and efonidipine showed IC₅₀ values of <40 μ M. Similarly, Jo et al.²⁸ screened a flavonoid library. Rhifolin, herbacetin, and pectolarin showed noteworthy inhibitory activity against M3CLpro. Khan et al.²⁹ screened anti-HIV drugs, and a traditional Chinese medicine (TCM) database to find that saquinavir and five TCM drugs could be promising leads against M3CLpro. In another study, Yang et al.³⁰ found that the anti-HIV drug darunavir has a good binding affinity for both COV-1 and COV-2 M3CLpro.

As part of this program, we have generated an *in silico* model of M3CLpro based on the X-ray crystal structure of this enzyme bound to boceprevir (PDB 7BRP, Figure 3).³¹ Boceprevir (4, Figure 1) was originally marketed as Victrelis by Schering-Plough (now Merck). It was FDA approved for the treatment of HCV in combination with peg-Interferon

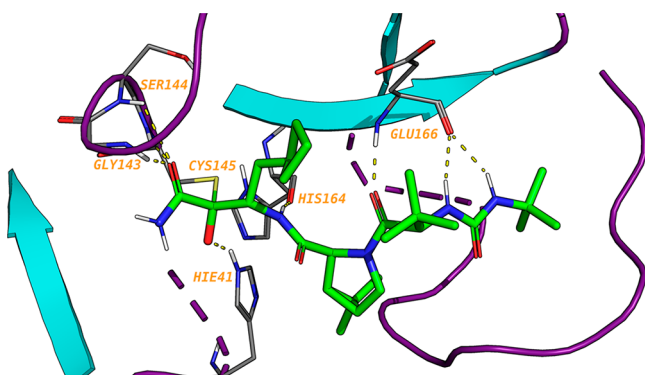


Figure 3. Boceprevir bound to M3CLpro (PDB 7BRP). Hydrogen bonds with key amino acids are shown as broken yellow lines.

and ribavirin (2011) but was supplanted by treatments such as Harvoni and Epclusa that are more effective in eliminating HCV infection. Interestingly, boceprevir is one of the few drugs employed as a mixture of diastereomers, as the chiral center (C3) of the 3-amino-4-cyclobutyl-2-oxobutanamide residue is configurationally unstable *in vivo*, and hence it exists as a mixture of two interconvertible diastereomers.^{32,33}

The X-ray crystal structure shows that the compound occupies the active site of M3CLpro, forms H-bonds with multiple residues (His⁴¹, Gly¹⁴³, Ser¹⁴⁴, His¹⁶⁴, Glu¹⁶⁶), and covalently binds to Cys¹⁴⁵.³¹

Herein, molecular dynamics (MD) simulations were performed to investigate the dynamic changes of the ligand binding site. Solvent mapping was carried out to compute the binding free energy of water molecules at the M3CLpro binding site. Various known HCV inhibitors were then tested *in vitro* against M3CLpro. On the basis of the present experimental results, asunaprevir, narlaprevir, paritaprevir, simeprevir, and telaprevir were selected for further computational analysis, with the use of molecular docking and MD simulations. The water free energy maps and MD simulations provide improved understanding of ligand recognition, binding site dynamics, and the role of ligand-interacting amino acid residues, which could aid in the rational design of therapeutics targeting M3CLpro.

METHODS

Protein Preparation for Molecular Dynamics Simulation. The crystal structure of boceprevir in complex with M3CLpro (PDB 7BRP) was obtained from the Protein Data Bank. The protein–ligand structures were prepared using the Protein Preparation Wizard (PrepWizard)^{34,35} workflow of the Schrödinger suite. With the use of Prime,^{36–38} missing residues and loops of M3CLpro were added. Appropriate protonation and tautomeric states were assigned for pH 7.0 ± 2.0. The original hydrogen atoms were removed, optimized hydrogen atoms were added, and water molecules beyond 5.0 Å of boceprevir were deleted. Next, hydrogen bonds were assigned, bond networks were optimized for pH 7.0, and water molecules with less than three hydrogen bonds to nonwater molecules were removed. The final structures were energy minimized with the OPLS3e force field with convergence of heavy atoms to an RMSD of 0.30 Å.

Docking of HCV Inhibitors. The binding site for HCV inhibitors was based on the bound position of boceprevir with protomer A of M3CLpro in the crystal structure. The binding site grid was prepared using Glide.^{39–42} Each ligand

was prepared for docking using LigPrep⁴³ with appropriate tautomers and stereoisomers assigned at pH 7.0 using Epik.^{44,45} Depending on the ligands different docking approaches were used: (i) For the covalently bound ligands, telaprevir and narlaprevir, binding modes were determined using a covalent docking approach. (ii) For noncovalently bound ligands, asunaprevir, simeprevir, and paritaprevir, a soft docking technique was used. Also, the Glide standard precision (SP) docking algorithm was used for asunaprevir, simeprevir, and paritaprevir. To allow for more receptor flexibility, softening the receptor potential was enabled by scaling the per-atom van der Waals radii and charges to 0.85. Cys¹⁴⁵ was selected as the reactive residue in the covalent docking of telaprevir and narlaprevir. The reaction type to nucleophilic addition with a double bond inserted to allow for the reactive group of the ligands to react with –SH of Cys¹⁴⁵. The docking poses were refined with Prime⁴⁰ by allowing flexibility of M3CLpro residues within 10 Å of the ligand. The ligand binding free energy (ΔG) of each pose was calculated using Prime MM-GBSA.⁴⁰ The binding mode with the lowest ΔG was then subjected to 100 ns MD simulation.

Molecular Dynamics Simulations. Table 1 provides the system details of MD simulations. After the docked

Table 1. System Details for MD Simulation of Different HCV Inhibitors Bound to M3CLpro

system	HCV inhibitor	simulation time (ns)	no. of atoms	no. of water atoms
covalently bound	boceprevir	400	83969	24861
	telaprevir	100	83934	24836
	narlaprevir	100	83951	24839
noncovalently bound	boceprevir	400	84022	24872
	asunaprevir	100	83885	24828
	simeprevir	100	83887	24828
	paritaprevir	100	83895	24831

conformation for other HCV inhibitors was selected, the system was solvated in a TIP3P⁴⁶ water box and neutralized with Na⁺ ions. All systems were run in DESMOND^{47,48} of the Schrödinger suite using the OPLS3e force field.⁴⁹ Systems were run in NPT ensemble with the constant pressure of 1 bar and the constant temperature of 300 K, using the Nosé–Hoover chain⁵⁰ and Martyna–Tobias–Klein coupling⁵¹ schemes, respectively. The RESPA integrator was employed in the numerical integration with a short-range/bonded interaction updated every 2 ps and long-range/nonbonded interactions updated every 6 ps.⁵² The short-range Coloumb interactions were calculated with a cutoff of 9.0 Å. Long-range interactions were calculated using the particle mesh Ewald method with a tolerance of 1×10^{-9} .⁵³ Images were generated using PyMOL²⁰ and VMD⁵⁴ visualization tools.

After the completion of each MD simulation run, the interaction strength is determined by quantifying the incidence of appearances in the trajectory using the simulation interaction diagram.^{47,48} The interaction fraction represents a normalized value of the number of times an interaction between a residue and ligand exists over the course of simulation.

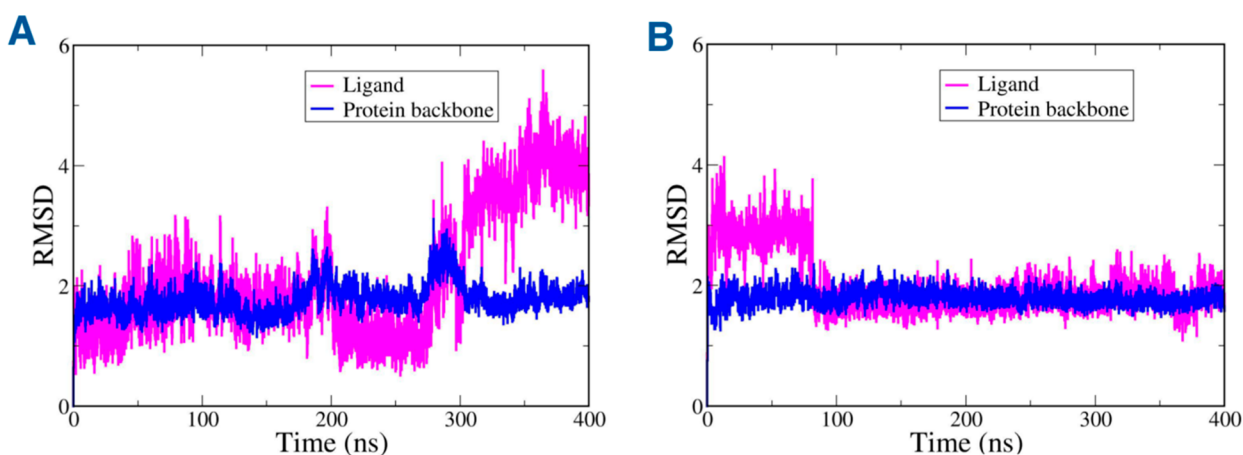


Figure 8. RMSD of boceprevir (magenta) and M3CLpro (blue) during 400 ns simulation of (A) boceprevir covalently bound with M3CLpro and (B) boceprevir noncovalently bound with M3CLpro.

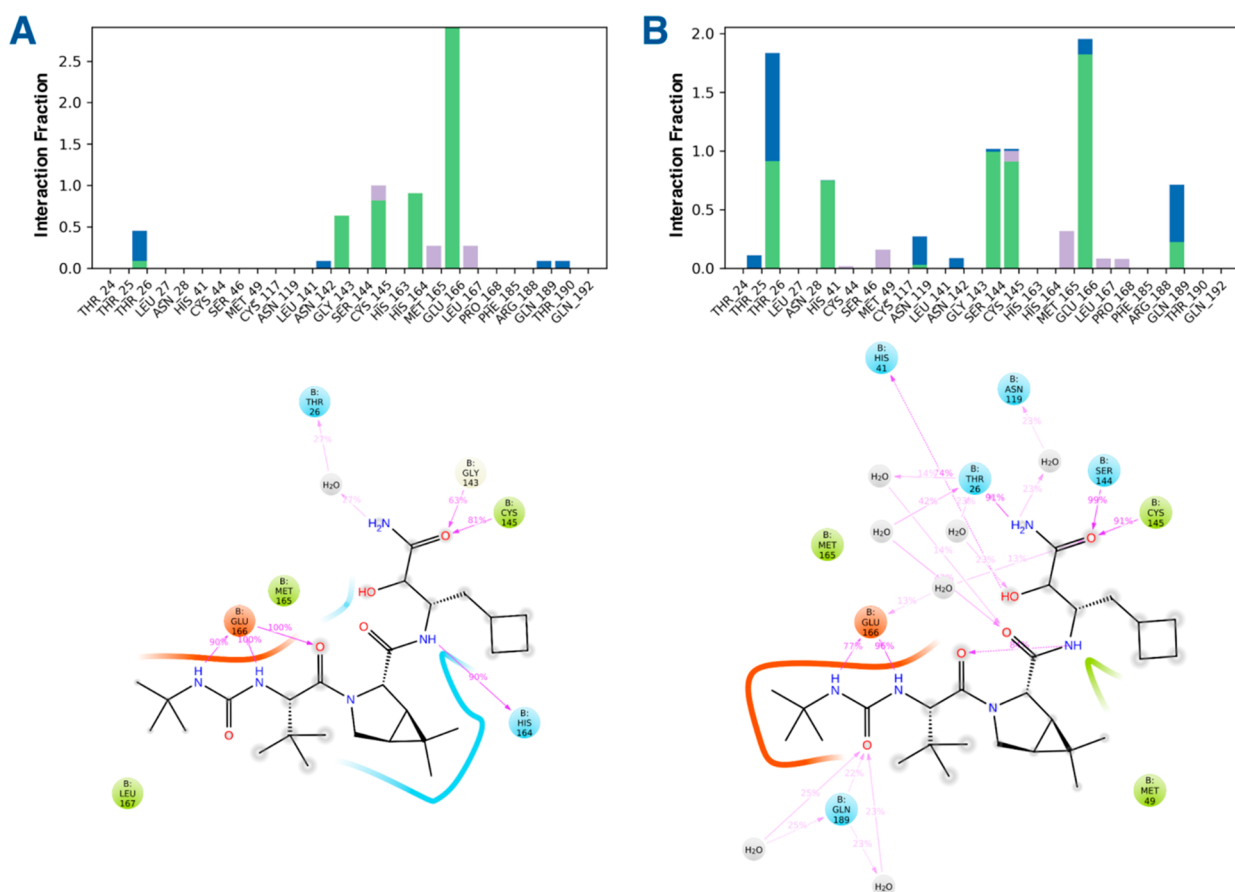


Figure 9. Interaction fraction (top panel) and 2D interaction diagram (lower panel) of covalently bound boceprevir with M3CLpro during (A) initial 1 ns and (B) last 100 ns.

blank value was subtracted from all values. IC_{50} 's and Hill fits were determined using a four-parameter fit, variable-slope equation, using GraphPad Prism.

RESULTS

M3CLpro Active Site. The active site of M3CLpro is located in the cleft between domain I and domain II and constitutes a catalytic dyad of Cys¹⁴⁵–His⁴¹ (Figure 2). Our model (Figure 4) shows that the terminal *tert*-butyl urea of boceprevir points into a large hydrophobic pocket, both the

cyclobutyl side chain and the central *tert*-butyl amino acid side chain are solvent exposed, and the proline ring system occupies a hydrophobic pocket. The binding pocket is composed mainly of polar residues including Thr²⁵, Thr²⁶, His⁴¹, Asn¹¹⁹, Asn¹⁴², Ser¹⁴⁴, Cys¹⁴⁵, and Gln¹⁸⁹; some hydrophobic residues such as Met⁴⁹, Met¹⁶⁵, Leu¹⁶⁷, and Pro¹⁶⁸, and a charged Glu¹⁶⁶.

Active Site Hydration. Protein–ligand binding takes place in an aqueous medium, so it is important to consider the effect of active site water molecules on ligand binding.

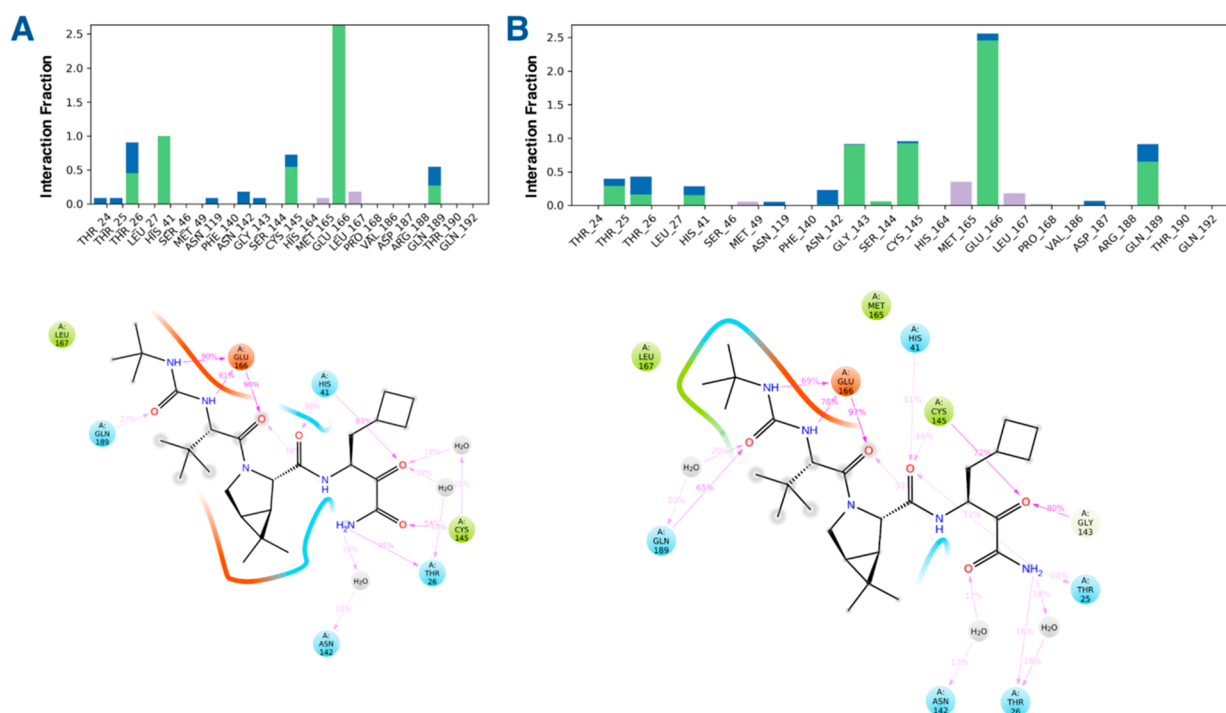


Figure 10. Interaction fraction (top panel) and 2D interaction diagram (lower panel) of noncovalently bound boceprevir with M3CLpro during (A) initial 1 ns and (B) last 100 ns.

Therefore, the hydration sites were mapped computationally over the surface of M3CLpro using SZMAP⁵⁵ (solvent-Zap-mapping), a semiexplicit solvent mapping technique. The net free energy of desolvation (dehydration) of the protein and ligand is a good indicator of the favorable and unfavorable contribution to protein–ligand binding. The binding free energies for water molecules in the binding sites were computed to identify positive (unfavorable) and negative (favorable) hydration sites. Water molecules in favorable hydration sites are tightly bound in the complex with strong electrostatic interactions, while unfavorable hydration sites show weak electrostatic interactions. It is necessary to identify these regions in the binding site to improve ligand design. Analysis of the binding site showed a pronounced stable hydration shell close to the side chains of Glu¹⁶⁶ and His¹⁷². A cluster of water molecules of negative free energy is located at this site with ΔG in the range -8.1 to -4.7 kcal/mol. Two smaller stable hydration sites are present: the first is close to the backbone of Glu¹⁶⁶ and side chain of Met¹⁶⁵; the second is close to Asn¹⁴², Gly¹⁴³, and Cys¹⁴⁵. These clusters (Figure 5) define the areas at which polar ligand groups could replace or interact with the solvent to enhance binding affinity, while hydrophobic groups would hurt binding. Boceprevir exploits the chemistry of the active site and replaces 12 water molecules with its polar atoms (oxygen and nitrogen atoms). An electrostatic mismatch was identified, however, as the *tert*-butyl group replaces a stable water molecule (W1, Figure 5B).

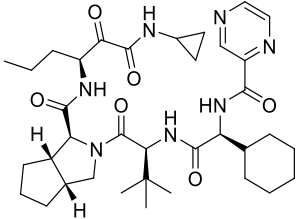
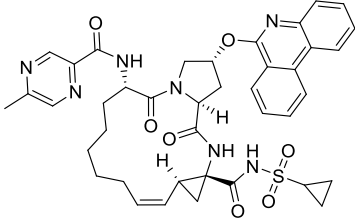
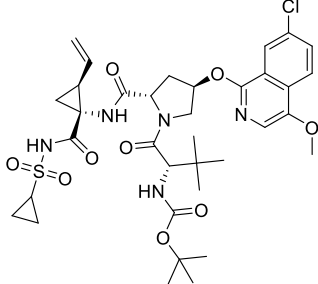
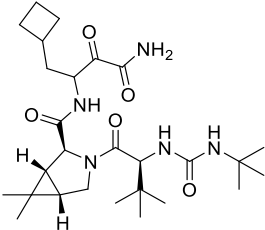
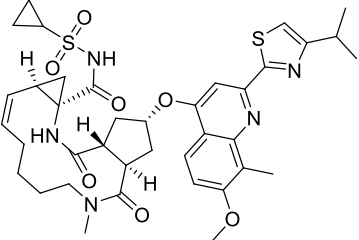
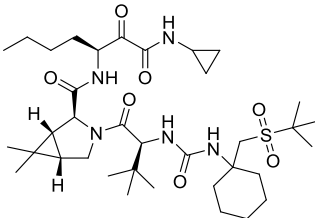
Positive free energy hydration sites were identified throughout the binding site (Figure 6), with a major cluster of unfavorable hydration shell in the region surrounded by His⁴¹, Met⁴⁹, His¹⁶⁴, and Asp¹⁸⁷. The free energy of these unstable hydration sites ranged from 0.8 to 2.1 kcal/mol. Hydrophobic ligand groups at these sites should improve the

binding affinity. The nonpolar groups of boceprevir are well-mapped with these regions.

MD Simulations. In order to develop a better understanding of boceprevir's interactions with M3CLpro, two molecular dynamics (MD) simulations were performed. The first MD system was constructed with the covalently bound boceprevir, and in the second system, the covalent bond between boceprevir and Cys¹⁴⁵ was broken. Analysis of the MD simulations showed that in the first system the loop composed of amino acid residues of 186–198 covering the substituted urea moiety of boceprevir moved away from its original position at the end of MD simulation (Figure S1). As shown in Figure 7A,B, shifting of this loop caused Gln¹⁸⁹ to lose its hydrogen bonding with the urea oxygen of the boceprevir. The initial distance between the centers of mass (COMs) of Gln¹⁸⁹ and urea oxygen increased from ~ 5 to ~ 12 Å by the end of MD simulation (Figure S2). Although the hydrogen bonding was lost, Gln¹⁸⁹ maintained water-mediated interactions with boceprevir. The loop opening facilitated access of water molecules between the loop and boceprevir (Figure 7A,B). The average number of water molecules was monitored within 8 Å of Met¹⁶⁵ and was found to be ~ 10 at the start of the simulation, which increased to ~ 15 after loop opening.

First, the initial 1 ns and last 100 ns of the 400 ns MD simulations of M3CLpro–boceprevir complex in both systems were compared to investigate the effect of covalent bonding on the dynamic behavior of inhibitor binding. The main protease was stable throughout the simulation time of both systems. In the first system, the RMSD of boceprevir increased ~ 290 ns (Figure 8A). The amino acid residues that interact with boceprevir were monitored throughout the MD simulation time (Figure 9). During the first 1 ns of the MD simulations, Glu¹⁶⁶ showed the strongest interactions, while Cys¹⁴⁵, His¹⁶⁴, Gly¹⁴³, and Thr²⁶ demonstrated weaker

Table 2. IC₅₀ Results of Selected HCV NS3/4a Protease Inhibitors Using the BPS BioScience M3CLpro (SARS-CoV-2) Assay Kit Using Untagged Enzyme

HCVNS3/4a inhibitor (M3CLpro IC ₅₀ (μM))	
 <p>Telaprevir (47.4)</p>	 <p>Paritaprevir (44.4)</p>
 <p>Asunaprevir (77.4)</p>	 <p>Boceprevir (8.9)</p>
 <p>Simeprevir (48.2)</p>	 <p>Narlaprevir (6.1)</p>

interactions. During the last 100 ns, boceprevir's interactions with Glu¹⁶⁶ and Thr²⁶ were stronger relative to boceprevir's interactions with Gly¹⁴³, Ser¹⁴⁴, His⁴¹, and Gln¹⁸⁹. The total contacts of M3CLpro with boceprevir increased throughout the course of MD simulation (Figure S3) and in particular during the last 100 ns, which could be correlated to the increase of ligand RMSD at ~290 ns. Significant conformational changes (Figure S4) were observed in loops I (residues 139–144), II (residues 165–173), and III (residues 189–195) by the end of the 400 ns. Loop I had moved outward, loop II demonstrated an upward shift, and loop III had inwardly relocated. Boceprevir displayed a slight movement toward loop III and away from loop I.

Next, key amino acid residues were inspected at different time frames. Interestingly, at ~290 ns the contacts between Gly¹⁴³ and His¹⁶⁴ with boceprevir diminished, while the contacts of Ser¹⁴⁴ and Thr²⁶ with boceprevir intensified (Figure S5). At ~275 ns, boceprevir showed hydrogen bonds with His¹⁶⁴ and Gly¹⁴³. At ~300 ns, boceprevir lost these interactions and formed a hydrogen bond with Ser¹⁴⁴. At

~310 ns, the azabicyclic ring of boceprevir had shifted upward, and boceprevir exhibited hydrogen bonds with Thr²⁶ and Ser¹⁴⁴ until the end of the 400 ns MD simulation. Starting from ~290 ns until the end of MD simulations, the distance between the C_α of Thr²⁵ and the amine of azabicyclic ring had been decreased from ~12 to ~6 Å (Figure S6).

In the second system boceprevir's RMSD decreased at ~80 ns and remained stable (Figure 8B). The same amino acid residues interacted with boceprevir throughout the MD simulation (Figure 10). Moreover, the interaction strengths of these amino acid residues with boceprevir were similar in the beginning and at the end of the simulation. Glu¹⁶⁶ had the most dominant and stable interactions with boceprevir throughout the MD simulation time. The same amino acid residue participated in three hydrogen bonds with boceprevir. The interaction of Gly¹⁴³ with boceprevir increased significantly in the last 100 ns compared to the initial 1 ns, whereas His⁴¹ experienced a 50% decrease in hydrogen bonding during the last 100 ns. Compared to system 1, there

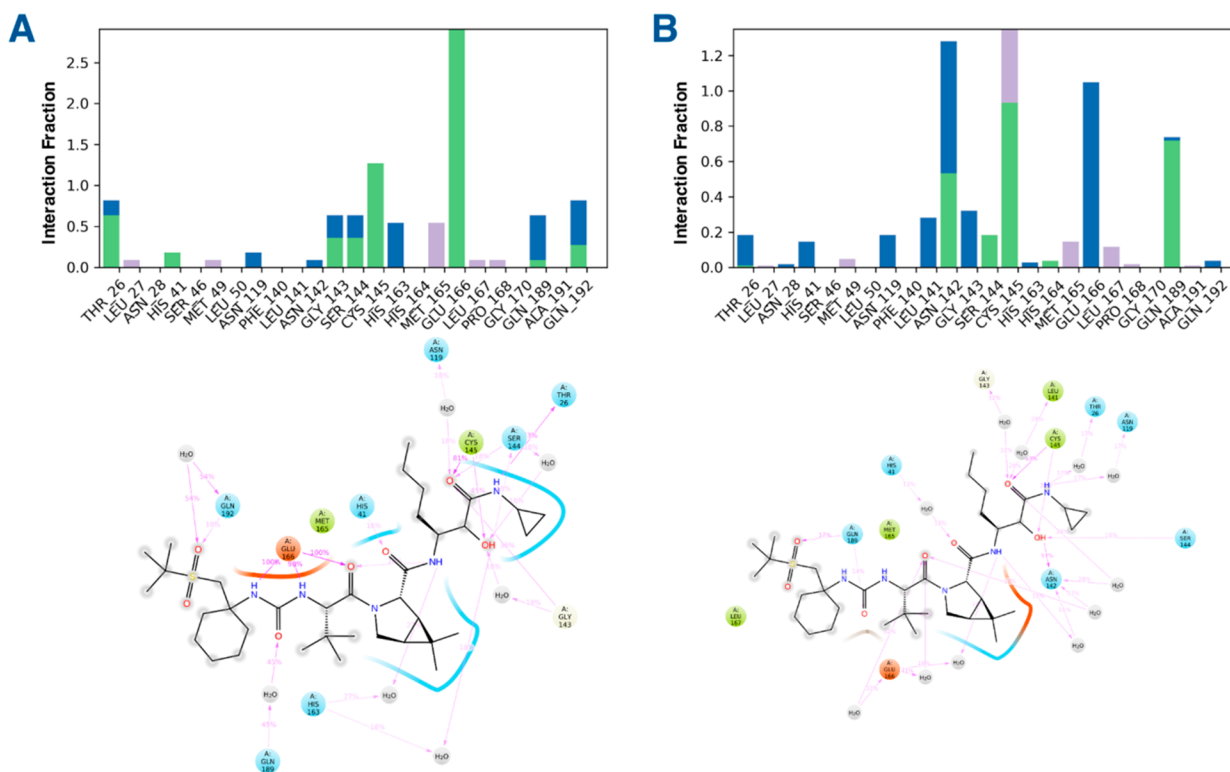


Figure 11. Interaction fraction (top panel) and 2D interaction diagram (lower panel) of narlaprevir bound with M3CLpro during (A) initial 1 ns and (B) last 10 ns.

were no significant changes in the positions of boceprevir and the loops around the binding cavity by the end of 400 ns simulation (Figure S4B). In general, covalently bound boceprevir (the first system) interacts with more residues with greater magnitude of binding compared to noncovalently bound boceprevir (the second system), which explains in part why covalently bound boceprevir is the favorable binding mode.

In Vitro Screening. As part of our effort to develop therapeutics to address the COVID-19 crisis, several HCV protease inhibitors were tested *in vitro* against M3CLpro (Table 2, Figure S7). Boceprevir inhibited M3CLpro with an IC_{50} of 8.9 μM . The measured IC_{50} value of boceprevir is similar to the recently published value ($8.0 \pm 1 \mu M$) reported by Fu et al.;³¹ however it is twice the value (4.13 μM , 5.1 μM) reported by Ma et al.⁵⁶ and Kneller et al.⁵⁷ Other NS3/4a protease inhibitors showed variable activities, with narlaprevir being the most potent with an IC_{50} of 6.1 μM and asunaprevir being the least active at 77.4 μM .

DISCUSSION

As already mentioned, the binding modes of telaprevir and narlaprevir were simulated via a covalent docking approach, while asunaprevir, simeprevir, and paritaprevir were investigated using soft docking techniques. MD simulations were analyzed to investigate the dynamic motion of M3CLpro at the atomic level in response to ligand binding. The M3CLpro for each system was stable throughout the 100 ns MD simulation (Figure S8).

Simeprevir. Gln¹⁸⁹, Glu¹⁶⁶, and Met¹⁶⁵ showed the most abundant contacts with simeprevir during the initial 1 ns and last 10 ns of the 100 ns MD simulation (Figure S9). During the last 10 ns, while the interactions of simeprevir with Glu¹⁶⁶

decreased, its interactions with Gln¹⁸⁹ increased. During the initial stage of MD simulation, Glu¹⁶⁶ interacted with simeprevir through one hydrogen bond for less than 10% of the simulation time. This hydrogen bond was lost at the last 10 ns. In addition, during the initial 1 ns of MD simulation, simeprevir showed multiple water-mediated hydrogen bonds with Gln¹⁸⁹ for a short fraction of time, which resulted in fewer but more stable interactions at the last 10 ns stage. The hydrogen bond between Gln¹⁸⁹ and simeprevir was lost at the final stage of MD simulations, and instead stable water-mediated hydrogen bonds were created.

Paritaprevir. For paritaprevir, Glu¹⁶⁶ showed the most dominant interactions followed by Asn¹⁴² and Phe¹⁴⁰ (Figure S10). Specifically, Glu¹⁶⁶ maintained multiple hydrogen bonds and water-bridged hydrogen bonds with paritaprevir throughout the course of the MD simulation. Both Asn¹⁴² and Phe¹⁴⁰ demonstrated more contacts with paritaprevir during the last 10 ns.

Asunaprevir. In the case of asunaprevir, during the initial stage of the MD simulation, Glu¹⁶⁶, Gln¹⁸⁹, and Gln¹⁹² exhibited the strongest interactions (Figure S11). However, during the last 10 ns, Glu¹⁶⁶ and Gln¹⁸⁹ maintained their interactions, while Gln¹⁹¹ lost most of its contacts with asunaprevir. In addition, Glu¹⁶⁶ lost hydrogen bonds with asunaprevir and formed stable water-mediated hydrogen bonds.

Narlaprevir. The dominant interactions in the case of narlaprevir were with Glu¹⁶⁶, Gln¹⁸⁹, Ser¹⁴⁴, Cys¹⁴⁵, and Asn¹⁴² (Figure 11). These interactions reorganized over the course of the MD trajectory. Glu¹⁶⁶, for example, participated in multiple hydrogen bonds during the initial stage of the MD simulation, all of which were lost during the last 10 ns, and instead several water-mediated hydrogen bonds were formed.

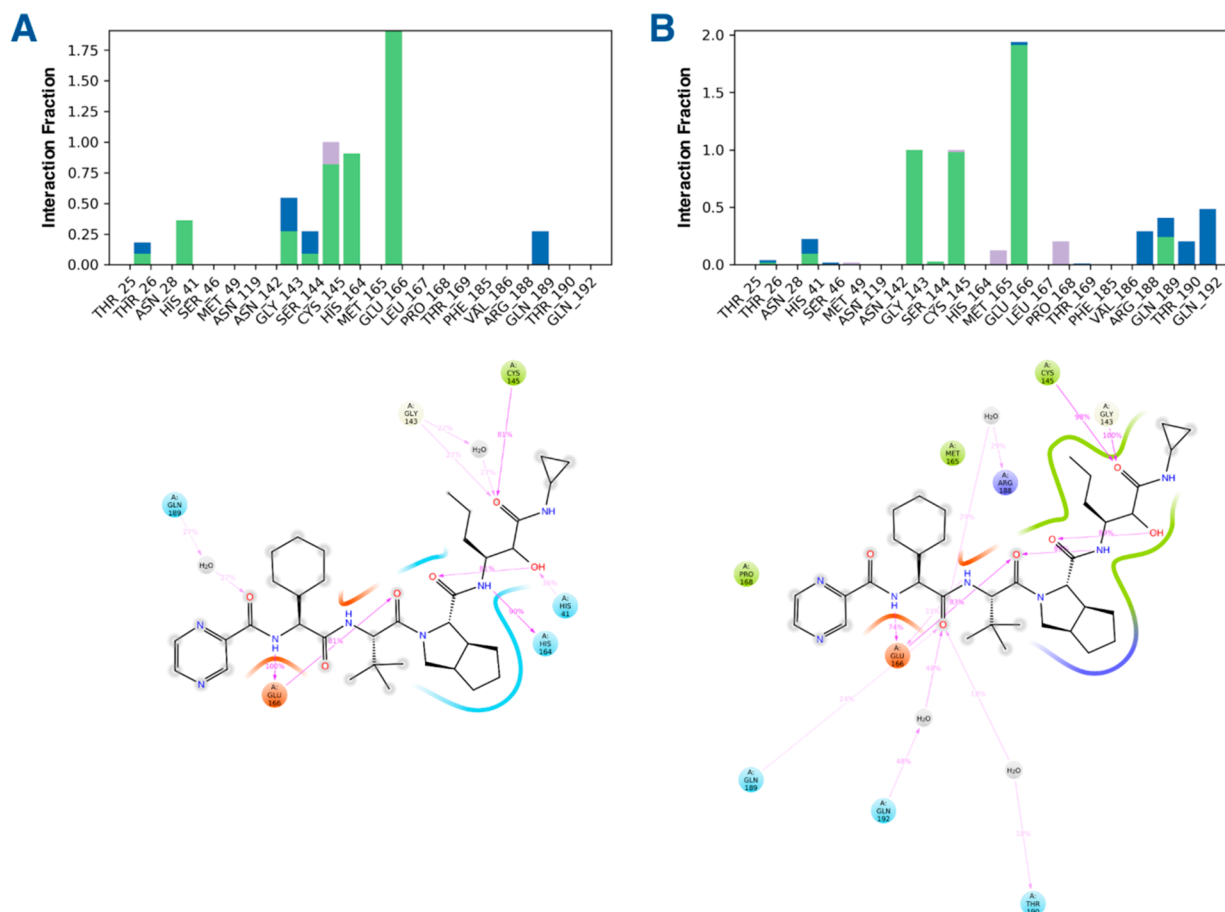


Figure 12. Interaction fraction (top panel) and 2D interaction diagram (lower panel) of telaprevir bound with M3CLpro during (A) initial 1 ns and (B) last 10 ns.

On the other hand, Gln¹⁸⁹ showed multiple water-bridged hydrogen bonds during the initial stages of the MD, which dissipated with concomitant development of strong hydrogen bonds over the last 10 ns. Cys¹⁴⁵ exhibited an additional hydrophobic contact during the last 10 ns, whereas Ser¹⁴⁴ lost all water-bridged hydrogen bonds. Asn¹⁴² showed more hydrogen bonding and water-bridged interactions in the last 10 ns.

Telaprevir. In the case of telaprevir, Glu¹⁶⁶, Cys¹⁴⁵, Gly¹⁴³, His¹⁶⁴, and His⁴¹ demonstrated the most abundant interactions (Figure 12). Here, protein–ligand interactions were homogeneous throughout the course of the MD simulation. Specifically, Glu¹⁶⁶ showed additional water-bridged hydrogen bonds during the last 10 ns, whereas His¹⁶⁴ and Ser¹⁴⁴ lost their interactions during the last 100 ns.

CONCLUSIONS

COVID-19 is a major threat to humankind, which demands the rapid discovery and development of novel antiviral therapies. The identification of novel therapeutics is, however, a time-consuming task. Given the hundreds of thousands of new cases and thousands of deaths reported every day, it is essential that new therapies be brought online as quickly as possible. Repurposing of previously approved drugs can significantly shorten the process by providing guidance on the possible reapplication of approved therapeutics and identifying potential starting points for new therapies. Computational tools can be employed to quickly and efficiently identify lead

compounds for *in vitro* and *in vivo* screening. Molecular modeling methods provide scientists with an understanding of drug–target interaction at the atomic level. The use of computational methods in combination with experimental methods can provide an efficiency boost in drug discovery, something that is desperately needed in the COVID-19 era.

We have employed molecular docking and MD simulations to explore the potential utility of FDA approved HCV drugs as inhibitors of M3CLpro. Our *in silico* studies indicate that covalent binding of boceprevir with M3CLpro is energetically favorable. Boceprevir initially showed strong interactions with Glu¹⁶⁶ and Cys¹⁴⁵, and after covalent binding, this compound developed strong interactions with Thr²⁶, Ser¹⁴⁴, and His⁴¹ as the MD simulations progressed. The binding free energy of water molecules at different locations of the binding site provided insight into the nature of the active site and the effect of different substitutions on ligand binding. The polar groups of boceprevir, for example, could displace water molecules near Glu¹⁶⁶ and His¹⁷², whereas nonpolar groups of boceprevir could displace water molecules near His⁴¹, Met⁴⁹, His¹⁶⁴, and Asp¹⁸⁷.

Other HCV inhibitors including simeprevir, paritaprevir, asunaprevir, telaprevir, and narlaprevir were tested *in vitro* against M3CLpro. Narlaprevir was the most potent with an IC₅₀ of 6.1 μM. Molecular modeling results suggest that all these inhibitors interact strongly with Glu¹⁶⁶. Covalent inhibitors telaprevir and narlaprevir showed stronger interactions compared to the noncovalent inhibitors simeprevir,

paritaprevir, and asunaprevir, particularly with Cys¹⁴⁵, Gly¹⁴³, and Asn¹⁴². The results of the MD simulations predict that narlaprevir binds stronger to M3CLpro than asunaprevir does, which agrees with the *in vitro* results.

Solvent mapping identified stable hydration sites near Glu¹⁶⁶; thus ligands with strong polar groups that can displace or interact with these water molecules would provide greater binding affinity. In summary, our findings indicate that it may be possible to develop M3CLpro inhibitors based on already known potent HCV protease inhibitors. Taking boceprevir as an example (Figure 13), regions A, B, and C

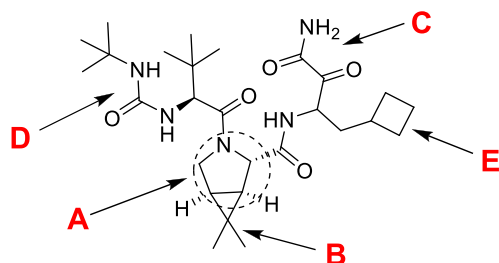


Figure 13. Possible modifications to improve the potency of boceprevir for M3CLpro.

play important roles in ligand binding. Region A can be modified to a small or a simple ring system, and B should be a slightly bulky substituent to fit into the hydrophobic cleft. Region C carries the warhead group to interact with Cys¹⁴⁵ and can be modified to hold the hydrogen bond donor/acceptor group for noncovalent binders. The *tert*-butyl group in D is not essential, and the cyclobutyl group can be modified to an alkyl or aromatic group substituted with a polar functional group.

■ ASSOCIATED CONTENT

SI Supporting Information

The Supporting Information is available free of charge at <https://pubs.acs.org/doi/10.1021/acs.jcim.0c01457>.

Comparison of loops composed of residues 186–198 in system 1 and system 2 of boceprevir–M3CLpro complex; distance between COMs of Gln189 and boceprevir covalently bound to M3CLpro; timeline of contacts M3CLpro makes with covalently bound boceprevir; comparison of 3D structures of system 1 and system 2 at the end of 1 and 400 ns; analysis of H-bonds of boceprevir with Thr²⁶, Gly¹⁴³, Ser¹⁴⁴, and His¹⁶⁴ in system 1; distance between C_α of Thr²⁵ and amine of azabicyclic ring of boceprevir; inhibition assay of HCV protease inhibitors against M3CLpro; RMSDs of M3CLpro backbone and HCV inhibitors; interaction fractions and 2D interaction diagrams of simeprevir, paritaprevir, and asunaprevir with M3CLpro; SMILES of boceprevir, telaprevir, narlaprevir, asunaprevir, simeprevir, and paritaprevir (PDF)

■ AUTHOR INFORMATION

Corresponding Author

Khaled M. Elokely – Institute for Computational Molecular Science and Department of Chemistry, Temple University, Philadelphia, Pennsylvania 19122, United States;

orcid.org/0000-0002-2394-021X; Email: kelokely@temple.edu

Authors

Anjela Manandhar – Institute for Computational Molecular Science and Department of Chemistry, Temple University, Philadelphia, Pennsylvania 19122, United States

Benjamin E. Blass – Department of Pharmaceutical Sciences, Moulder Center for Drug Discovery Research, Temple University School of Pharmacy, Philadelphia, Pennsylvania 19140, United States; orcid.org/0000-0003-2449-4503

Dennis J. Colussi – Department of Pharmaceutical Sciences, Moulder Center for Drug Discovery Research, Temple University School of Pharmacy, Philadelphia, Pennsylvania 19140, United States

Imane Almi – Department of Pharmaceutical Sciences, Moulder Center for Drug Discovery Research, Temple University School of Pharmacy, Philadelphia, Pennsylvania 19140, United States; Group of Computational and Pharmaceutical Chemistry, LMCE Laboratory, University of Biskra, Biskra 07000, Algeria

Magid Abou-Gharbia – Department of Pharmaceutical Sciences, Moulder Center for Drug Discovery Research, Temple University School of Pharmacy, Philadelphia, Pennsylvania 19140, United States; orcid.org/0000-0001-7524-6011

Michael L. Klein – Institute for Computational Molecular Science and Department of Chemistry, Temple University, Philadelphia, Pennsylvania 19122, United States

Complete contact information is available at:

<https://pubs.acs.org/doi/10.1021/acs.jcim.0c01457>

Author Contributions

B.E.B., D.J.C., M.A., and K.M.E. designed the research; A.M., I.A., and D.J.C. performed the research; A.M., B.E.B., D.J.C., I.A., M.A., M.L.K., and K.M.E. analyzed the data; and A.M., B.E.B., D.J.C., I.A., M.A., M.L.K., and K.M.E. wrote and revised the paper.

Notes

The authors declare no competing financial interest.

■ ACKNOWLEDGMENTS

We are grateful to OpenEye Scientific Software Inc. for providing us with an invaluable academic license to their software.

■ ABBREVIATIONS

SARS-CoV-2, severe acute respiratory syndrome coronavirus 2; M3CLpro, coronavirus main cysteine protease; MD, molecular dynamics; RMSD, root-mean-square deviation.

■ REFERENCES

- (1) Gorbalenya, A. E.; Baker, S. C.; Baric, R. S.; de Groot, R. J.; Drosten, C.; Gulyaeva, A. A.; Haagmans, B. L.; Lauber, C.; Leontovich, A. M.; Neuman, B. W.; Penzar, D.; Perlman, S.; Poon, L. L. M.; Samborskiy, D. V.; Sidorov, I. A.; Sola, I.; Ziebuhr, J. The Species Severe Acute Respiratory Syndrome-Related Coronavirus: Classifying 2019-NCoV and Naming It SARS-CoV-2. *Nat. Microbiol.* **2020**, *5*, 536–544.
- (2) Zhou, P.; Yang, X. L.; Wang, X. G.; Hu, B.; Zhang, L.; Zhang, W.; Si, H. R.; Zhu, Y.; Li, B.; Huang, C. L.; Chen, H. D.; Chen, J.; Luo, Y.; Guo, H.; Jiang, R. D.; Liu, M. Q.; Chen, Y.; Shen, X. R.; Wang, X.; Zheng, X. S.; Zhao, K.; Chen, Q. J.; Deng, F.; Liu, L. L.;

Yan, B.; Zhan, F. X.; Wang, Y. Y.; Xiao, G. F.; Shi, Z. L. A Pneumonia Outbreak Associated with a New Coronavirus of Probable Bat Origin. *Nature* **2020**, *579*, 270–273.

(3) Zhu, N.; Zhang, D.; Wang, W.; Li, X.; Yang, B.; Song, J.; Zhao, X.; Huang, B.; Shi, W.; Lu, R.; Niu, P.; Zhan, F.; Ma, X.; Wang, D.; Xu, W.; Wu, G.; Gao, G. F.; Tan, W. A Novel Coronavirus from Patients with Pneumonia in China, 2019. *N. Engl. J. Med.* **2020**, *382*, 727–733.

(4) Taubenberger, J. K.; Morens, D. M. 1918 Influenza: The Mother of All Pandemics. *Emerging Infect. Dis.* **2006**, *12*, 15–22.

(5) WHO Director-General's opening remarks at the media briefing on COVID-19 - 11 March 2020. World Health Organization, March 11, 2020. <https://www.who.int/director-general/speeches/detail/who-director-general-s-opening-remarks-at-the-media-briefing-on-covid-19--11-march-2020> (accessed 2020-11-11).

(6) Hilgenfeld, R.; Peiris, M. From SARS to MERS: 10 Years of Research on Highly Pathogenic Human Coronaviruses. *Antiviral Res.* **2013**, *100*, 286–295.

(7) Gumashta, J.; Gumashta, R. Role of the Backbenchers of the Renin-Angiotensin System ACE2 and AT2 Receptors in COVID-19: Lessons From SARS. *Cureus* **2020**, *12* (6), e8411.

(8) Zhang, H.; Penninger, J. M.; Li, Y.; Zhong, N.; Slutsky, A. S. Angiotensin-Converting Enzyme 2 (ACE2) as a SARS-CoV-2 Receptor: Molecular Mechanisms and Potential Therapeutic Target. *Intensive Care Med.* **2020**, *46*, 586–590.

(9) Wu, C.; Liu, Y.; Yang, Y.; Zhang, P.; Zhong, W.; Wang, Y.; Wang, Q.; Xu, Y.; Li, M.; Li, X.; Zheng, M.; Chen, L.; Li, H. Analysis of Therapeutic Targets for SARS-CoV-2 and Discovery of Potential Drugs by Computational Methods. *Acta Pharm. Sin. B* **2020**, *10*, 766–788.

(10) Shin, D.; Mukherjee, R.; Grewe, D.; Bojkova, D.; Baek, K.; Bhattacharya, A.; Schulz, L.; Widera, M.; Mehdi-pour, A. R.; Tascher, G.; Geurink, P. P.; Wilhelm, A.; van der Heden van Noort, G. J.; Ovaas, H.; Müller, S.; Knobeloch, K. P.; Rajalingam, K.; Schulman, B. A.; Cinatl, J.; Hummer, G.; Ciesek, S.; Dikic, I. Papain-like Protease Regulates SARS-CoV-2 Viral Spread and Innate Immunity. *Nature* **2020**, *587*, 657–662.

(11) Liu, C.; Zhou, Q.; Li, Y.; Garner, L. V.; Watkins, S. P.; Carter, L. J.; Smoot, J.; Gregg, A. C.; Daniels, A. D.; Jerve, S.; Albaiu, D. Research and Development on Therapeutic Agents and Vaccines for COVID-19 and Related Human Coronavirus Diseases. *ACS Cent. Sci.* **2020**, *6*, 315–331.

(12) Beigel, J. H.; Tomashek, K. M.; Dodd, L. E.; Mehta, A. K.; Zingman, B. S.; Kalil, A. C.; Hohmann, E.; Chu, H. Y.; Luetkemeyer, A.; Kline, S.; Lopez de Castilla, D.; Finberg, R. W.; Dierberg, K.; Tapson, V.; Hsieh, L.; Patterson, T. F.; Paredes, R.; Sweeney, D. A.; Short, W. R.; Touloumi, G.; Lye, D. C.; Ohmagari, N.; Oh, M.; Ruiz-Palacios, G. M.; Benfield, T.; Fätkenheuer, G.; Kortepeter, M. G.; Atmar, R. L.; Creech, C. B.; Lundgren, J.; Babiker, A. G.; Pett, S.; Neaton, J. D.; Burgess, T. H.; Bonnett, T.; Green, M.; Makowski, M.; Osinusi, A.; Nayak, S.; Lane, H. Remdesivir for the Treatment of Covid-19 — Final Report. *N. Engl. J. Med.* **2020**, *383*, 1813–1826.

(13) Coronavirus (COVID-19) update: FDA issues Emergency Use Authorization for potential COVID-19 treatment. Food and Drug Administration, August 28, 2020. <https://www.fda.gov/news-events/press-announcements/coronavirus-covid-19-update-fda-issues-emergency-use-authorization-potential-covid-19-treatment> (accessed 2020-11-20).

(14) Buckland, M. S.; Galloway, J. B.; Fhogartaigh, C. N.; Meredith, L.; Provine, N. M.; Bloor, S.; Ogbe, A.; Zelek, W. M.; Smielewska, A.; Yakovleva, A.; Mann, T.; Bergamaschi, L.; Turner, L.; Mescia, F.; Toonen, E. J. M.; Hackstein, C.-P.; Akther, H. D.; Vieira, V. A.; Ceron-Gutierrez, L.; Perisleris, J.; Kiani-Alikhan, S.; Grigoriadou, S.; Vaghela, D.; Lear, S. E.; Török, M. E.; Hamilton, W. L.; Stockton, J.; Quick, J.; Nelson, P.; Hunter, M.; Coulter, T. I.; Devlin, L.; Bradley, J. R.; Smith, K. G. C.; Ouwehand, W. H.; Estcourt, L.; Harvala, H.; Roberts, D. J.; Wilkinson, I. B.; Sreaton, N.; Loman, N.; Doffinger, R.; Lyons, P. A.; Morgan, B. P.;

Goodfellow, I. G.; Klenerman, P.; Lehner, P. J.; Matheson, N. J.; Thaventhiran, J. E. D. Treatment of COVID-19 with Remdesivir in the Absence of Humoral Immunity: A Case Report. *Nat. Commun.* **2020**, *11*, 6385.

(15) Gulick, R. M.; Mellors, J. W.; Havlir, D.; Eron, J. J.; Gonzalez, C.; McMahon, D.; Richman, D. D.; Valentine, F. T.; Jonas, L.; Meibohm, A.; Emini, E. A.; Chodakewitz, J. A.; Deutsch, P.; Holder, D.; Schleif, W. A.; Condra, J. Treatment with Indinavir, Zidovudine, and Lamivudine in Adults with Human Immunodeficiency Virus Infection and Prior Antiretroviral Therapy. *N. Engl. J. Med.* **1997**, *337*, 734–739.

(16) Hammer, S. M.; Squires, K. E.; Hughes, M. D.; Grimes, J. M.; Demeter, L. M.; Currier, J. S.; Eron, J. J.; Feinberg, J. E.; Balfour, H. H.; Deyton, L. R.; Chodakewitz, J. A.; Fischl, M. A.; Phair, J. P.; Pedneault, L.; Nguyen, B.-Y.; Cook, J. C. A Controlled Trial of Two Nucleoside Analogues plus Indinavir in Persons with Human Immunodeficiency Virus Infection and CD4 Cell Counts of 200 per Cubic Millimeter or Less. *N. Engl. J. Med.* **1997**, *337*, 725–733.

(17) Granich, R.; Crowley, S.; Vitoria, M.; Smyth, C.; Kahn, J. G.; Bennett, R.; Lo, Y. R.; Souteyrand, Y.; Williams, B. Highly Active Antiretroviral Treatment as Prevention of HIV Transmission: Review of Scientific Evidence and Update. *Curr. Opin. HIV AIDS* **2010**, *5*, 298–304.

(18) Wei, L.; Wang, G.; Alami, N. N.; Xie, W.; Heo, J.; Xie, Q.; Zhang, M.; Kim, Y. J.; Lim, S. G.; Fredrick, L. M.; Lu, W.; Liu, W.; Kalluri, H. V.; Krishnan, P.; Tripathi, R.; Mobashery, N.; Burroughs, M.; Asatryan, A.; Jia, J.; Hou, J. Glecaprevir–Pibrentasvir to Treat Chronic Hepatitis C Virus Infection in Asia: Two Multicentre, Phase 3 Studies— a Randomised, Double-Blind Study (VOYAGE-1) and an Open-Label, Single-Arm Study (VOYAGE-2). *Lancet Gastroenterol. Hepatol.* **2020**, *5*, 839–849.

(19) Kish, T.; Aziz, A.; Sorio, M. Hepatitis C in a New Era: A Review of Current Therapies. *P T* **2017**, *42*, 316–329.

(20) *The PyMOL Molecular Graphics System*, ver. 2.0; Schrödinger, LLC.

(21) Hilgenfeld, R. From SARS to MERS: Crystallographic Studies on Coronavirus Proteases Enable Antiviral Drug Design. *FEBS J.* **2014**, *281*, 4085–4096.

(22) Zhang, L.; Lin, D.; Sun, X.; Curth, U.; Drosten, C.; Sauerhering, L.; Becker, S.; Rox, K.; Hilgenfeld, R. Crystal Structure of SARS-CoV-2 Main Protease Provides a Basis for Design of Improved α -Ketoamide Inhibitors. *Science* **2020**, *368*, 409–412.

(23) Shi, J.; Song, J. The Catalysis of the SARS 3C-like Protease Is under Extensive Regulation by Its Extra Domain. *FEBS J.* **2006**, *273*, 1035–1045.

(24) Anand, K.; Palm, G. J.; Mesters, J. R.; Siddell, S. G.; Ziebuhr, J.; Hilgenfeld, R. Structure of Coronavirus Main Proteinase Reveals Combination of a Chymotrypsin Fold with an Extra α -Helical Domain. *EMBO J.* **2002**, *21*, 3213–3224.

(25) Siklos, M.; BenAissa, M.; Thatcher, G. R. J. Cysteine Proteases as Therapeutic Targets: Does Selectivity Matter? A Systematic Review of Calpain and Cathepsin Inhibitors. *Acta Pharm. Sin. B* **2015**, *5*, 506–519.

(26) Boras, B.; Jones, R. M.; Anson, B. J.; Arenson, D.; Aschenbrenner, L.; Bakowski, M. A.; Beutler, N.; Binder, J.; Chen, E.; Eng, H.; Hammond, J.; Hoffman, R.; Kadar, E. P.; Kania, R.; Kimoto, E.; Kirkpatrick, M. G.; Lanyon, L.; Lendy, E. K.; Lillis, J. R.; Luthra, S. A.; Ma, C.; Noell, S.; Obach, R. S.; O'Brien, M. N.; O'Connor, R.; Ogilvie, K.; Owen, D.; Pettersson, M.; Reese, M. R.; Rogers, T.; Rossulek, M. I.; Sathish, J. G.; Steppan, C.; Ticehurst, M.; Updyke, L. W.; Zhu, Y.; Wang, J.; Chatterjee, A. K.; Mesecar, A. D.; Anderson, A. S.; Allerton, C. Discovery of a Novel Inhibitor of Coronavirus 3CL Protease as a Clinical Candidate for the Potential Treatment of COVID-19. *bioRxiv*. September 13, 2020, 2020.09.12.293498, ver. 2. <https://www.biorxiv.org/content/10.1101/2020.09.12.293498v2>.

(27) Ghahremanpour, M. M.; Tirado-Rives, J.; Deshmukh, M.; Ippolito, J. A.; Zhang, C. H.; Cabeza De Vaca, I.; Liosi, M. E.; Anderson, K. S.; Jorgensen, W. L. Identification of 14 Known Drugs

as Inhibitors of the Main Protease of SARS-CoV-2. *ACS Med. Chem. Lett.* **2020**, *11*, 2526–2533.

(28) Jo, S.; Kim, S.; Shin, D. H.; Kim, M. S. Inhibition of SARS-CoV 3CL Protease by Flavonoids. *J. Enzyme Inhib. Med. Chem.* **2020**, *35*, 145–151.

(29) Khan, A.; Ali, S. S.; Khan, M. T.; Saleem, S.; Ali, A.; Suleman, M.; Babar, Z.; Shafiq, A.; Khan, M.; Wei, D. Q. Combined Drug Repurposing and Virtual Screening Strategies with Molecular Dynamics Simulation Identified Potent Inhibitors for SARS-CoV-2 Main Protease (3CLpro). *J. Biomol. Struct. Dyn.* **2020**, 1–12.

(30) Sang, P.; Tian, S. H.; Meng, Z. H.; Yang, L. Q. Anti-HIV Drug Repurposing against SARS-CoV-2. *RSC Adv.* **2020**, *10*, 15775–15783.

(31) Fu, L.; Ye, F.; Feng, Y.; Yu, F.; Wang, Q.; Wu, Y.; Zhao, C.; Sun, H.; Huang, B.; Niu, P.; Song, H.; Shi, Y.; Li, X.; Tan, W.; Qi, J.; Gao, G. F. Both Boceprevir and GC376 Efficaciously Inhibit SARS-CoV-2 by Targeting Its Main Protease. *Nat. Commun.* **2020**, *11*, 4417.

(32) *Clinical Pharmacology and Biopharmaceutics Review*; Center for Drug Evaluation and Research, April 20, 2011. https://www.accessdata.fda.gov/drugsatfda_docs/nda/2011/202258Orig1s000ClinPharmR.pdf (accessed 2020-11-20).

(33) Kiser, J. J.; Burton, J. R.; Anderson, P. L.; Everson, G. T. Review and Management of Drug Interactions with Boceprevir and Telaprevir. *Hepatology* **2012**, *55*, 1620–1628.

(34) Madhavi Sastry, G.; Adzhigirey, M.; Day, T.; Annabhimoju, R.; Sherman, W. Protein and Ligand Preparation: Parameters, Protocols, and Influence on Virtual Screening Enrichments. *J. Comput.-Aided Mol. Des.* **2013**, *27*, 221–234.

(35) Protein Preparation Wizard. Epik. *Schrödinger Release 2018-4*; Schrödinger, LLC: New York, NY, 2020. Impact. *Schrödinger, LLC*: New York, NY, 2018. Prime. *Schrödinger, LLC*: New York, NY, 2018.

(36) Jacobson, M. P.; Friesner, R. A.; Xiang, Z.; Honig, B. On the Role of the Crystal Environment in Determining Protein Side-Chain Conformations. *J. Mol. Biol.* **2002**, *320*, 597–608.

(37) Jacobson, M. P.; Pincus, D. L.; Rapp, C. S.; Day, T. J. F.; Honig, B.; Shaw, D. E.; Friesner, R. A. A Hierarchical Approach to All-Atom Protein Loop Prediction. *Proteins: Struct., Funct., Genet.* **2004**, *55*, 351–367.

(38) Prime. *Schrödinger Release 2018-4*; Schrödinger, LLC, New York, NY, 2018.

(39) Glide. *Schrödinger Release 2018-4*; Schrödinger, LLC: New York, NY, 2018.

(40) Friesner, R. A.; Banks, J. L.; Murphy, R. B.; Halgren, T. A.; Klicic, J. J.; Mainz, D. T.; Repasky, M. P.; Knoll, E. H.; Shelley, M.; Perry, J. K.; Shaw, D. E.; Francis, P.; Shenkin, P. S. Glide: A New Approach for Rapid, Accurate Docking and Scoring. 1. Method and Assessment of Docking Accuracy. *J. Med. Chem.* **2004**, *47*, 1739–1749.

(41) Halgren, T. A.; Murphy, R. B.; Friesner, R. A.; Beard, H. S.; Frye, L. L.; Pollard, W. T.; Banks, J. L. Glide: A New Approach for Rapid, Accurate Docking and Scoring. 2. Enrichment Factors in Database Screening. *J. Med. Chem.* **2004**, *47*, 1750–1759.

(42) Friesner, R. A.; Murphy, R. B.; Repasky, M. P.; Frye, L. L.; Greenwood, J. R.; Halgren, T. A.; Sanschagrin, P. C.; Mainz, D. T. Extra Precision Glide: Docking and Scoring Incorporating a Model of Hydrophobic Enclosure for Protein-Ligand Complexes. *J. Med. Chem.* **2006**, *49*, 6177–6196.

(43) LigPrep. *Schrödinger Release 2018-4*; Schrödinger, LLC: New York, NY, 2018.

(44) Shelley, J. C.; Cholleti, A.; Frye, L. L.; Greenwood, J. R.; Timlin, M. R.; Uchimaya, M. Epik: A Software Program for PKa Prediction and Protonation State Generation for Drug-like Molecules. *J. Comput.-Aided Mol. Des.* **2007**, *21*, 681–691.

(45) Greenwood, J. R.; Calkins, D.; Sullivan, A. P.; Shelley, J. C. Towards the Comprehensive, Rapid, and Accurate Prediction of the Favorable Tautomeric States of Drug-like Molecules in Aqueous Solution. *J. Comput.-Aided Mol. Des.* **2010**, *24*, 591–604.

(46) Jorgensen, W. L.; Chandrasekhar, J.; Madura, J. D.; Impey, R. W.; Klein, M. L. Comparison of Simple Potential Functions for Simulating Liquid Water. *J. Chem. Phys.* **1983**, *79*, 926–935.

(47) Bowers, K. J.; Chow, E.; Xu, H.; Dror, R. O.; Eastwood, M. P.; Gregersen, B. A.; Klepeis, J. L.; Kolossvary, I.; Moraes, M. A.; Sacerdoti, F. D.; Salmon, J. K.; Shan, Y.; Shaw, D. E. Scalable Algorithms for Molecular Dynamics Simulations on Commodity Clusters. In *Proceedings of the 2006 ACM/IEEE Conference on Supercomputing, SC'06*; ACM Press: New York, NY, 2006; p 84.

(48) *Schrödinger Release 2018-4; Desmond Molecular Dynamics System*; D. E. Shaw Research: New York, NY, 2020. *Maestro-Desmond Interoperability Tools*; Schrödinger: New York, NY, 2018.

(49) Harder, E.; Damm, W.; Maple, J.; Wu, C.; Reboul, M.; Xiang, J. Y.; Wang, L.; Lupyán, D.; Dahlgren, M. K.; Knight, J. L.; Kaus, J. W.; Cerutti, D. S.; Krilov, G.; Jorgensen, W. L.; Abel, R.; Friesner, R. A. OPLS3: A Force Field Providing Broad Coverage of Drug-like Small Molecules and Proteins. *J. Chem. Theory Comput.* **2016**, *12*, 281–296.

(50) Martyna, G. J.; Tobias, D. J.; Klein, M. L. Constant Pressure Molecular Dynamics Algorithms. *J. Chem. Phys.* **1994**, *101*, 4177–4189.

(51) Martyna, G. J.; Klein, M. L.; Tuckerman, M. Nosé-Hoover Chains: The Canonical Ensemble via Continuous Dynamics. *J. Chem. Phys.* **1992**, *97*, 2635–2643.

(52) Tuckerman, M. E.; Berne, B. J.; Rossi, A. Molecular Dynamics Algorithm for Multiple Time Scales: Systems with Disparate Masses. *J. Chem. Phys.* **1991**, *94*, 1465–1469.

(53) Toukmaji, A. Y.; Board, J. A. Ewald Summation Techniques in Perspective: A Survey. *Comput. Phys. Commun.* **1996**, *95*, 73–92.

(54) Humphrey, W.; Dalke, A.; Schulten, K. VMD: Visual Molecular Dynamics. *J. Mol. Graphics* **1996**, *14*, 33–38.

(55) SZMAP 1.6.0.4; OpenEye Scientific Software: Santa Fe, NM, 2013. <http://www.eyesopen.com> (accessed 2020-11-11).

(56) Ma, C.; Sacco, M. D.; Hurst, B.; Townsend, J. A.; Hu, Y.; Szeto, T.; Zhang, X.; Tarbet, B.; Marty, M. T.; Chen, Y.; Wang, J. Boceprevir, GC-376, and Calpain Inhibitors II, XII Inhibit SARS-CoV-2 Viral Replication by Targeting the Viral Main Protease. *Cell Res.* **2020**, *30* (8), 678–692.

(57) Kneller, D. W.; Galanie, S.; Phillips, G.; O'Neill, H. M.; Coates, L.; Kovalevsky, A. Malleability of the SARS-CoV-2 3CL Mpro Active-Site Cavity Facilitates Binding of Clinical Antivirals. *Structure* **2020**, *28*, 1313.